e-ISSN 2150-5551
CN 31-2103/TB

Nano-Micro Letters

ARTICLE https://doi.org/10.1007/s40820-024-01342-3

Cite as
Nano-Micro Lett.
(2024) 16:126

Received: 12 October 2023
Accepted: 3 January 2024
© The Author(s) 2024

On-Chip Micro Temperature Controllers Based on Freestanding Thermoelectric Nano Films for Low-Power Electronics

Qun Jin[1] ✉, Tianxiao Guo[2], Nicolás Pérez[1], Nianjun Yang[2], Xin Jiang[2], Kornelius Nielsch[1,3,4] ✉, Heiko Reith[1] ✉

HIGHLIGHTS

- Dense and flat freestanding Bi_2Te_3-based thermoelectric nano films were successfully fabricated by sputtering technology using a newly developed nano graphene oxide membrane as a substrate.
- On-chip micro temperature controllers were integrated using conventional micro-electromechanical system technology, to achieve energy-efficient temperature control for low-power electronics.
- The tunable equivalent thermal resistance enables an ultrahigh temperature control capability of 100 K mW^{-1} and an ultra-fast cooling rate exceeding 2000 K s^{-1}, as well as excellent reliability of up to 1 million cycles.

ABSTRACT Multidimensional integration and multifunctional component assembly have been greatly explored in recent years to extend Moore's Law of modern microelectronics. However, this inevitably exacerbates the inhomogeneity of temperature distribution in microsystems, making precise temperature control for electronic components extremely challenging. Herein, we report an on-chip micro temperature controller including a pair of thermoelectric legs with a total area of 50×50 μm^2, which are fabricated from dense and flat freestanding Bi_2Te_3-based thermoelectric nano films deposited on a newly developed nano graphene oxide membrane substrate. Its tunable equivalent thermal resistance is controlled by electrical currents to achieve energy-efficient temperature control for low-power electronics. A large cooling temperature difference of 44.5 K at 380 K is achieved with a power consumption of only 445 μW, resulting in an ultrahigh temperature control capability over 100 K mW^{-1}. Moreover, an ultra-fast cooling rate exceeding 2000 K s^{-1} and excellent reliability of up to 1 million cycles are observed. Our proposed on-chip temperature controller is expected to enable further miniaturization and multifunctional integration on a single chip for microelectronics.

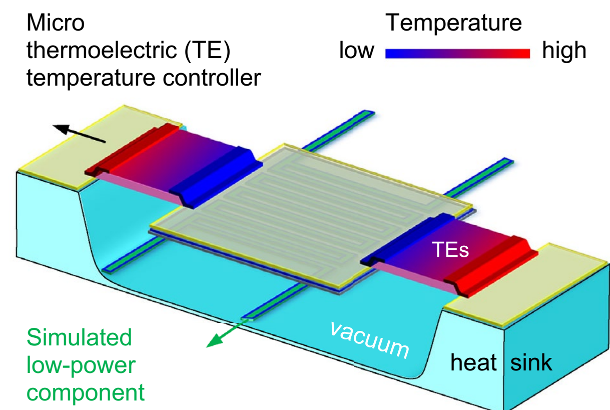

KEYWORDS Temperature control; Low-power electronics; On-chip micro temperature controller; Freestanding thermoelectric nano films; Temperature-sensitive components

✉ Qun Jin, q.jin@ifw-dresden.de; Kornelius Nielsch, k.nielsch@ifw-dresden.de; Heiko Reith, h.reith@ifw-dresden.de
[1] Institute for Metallic Materials, Leibniz Institute for Solid State and Materials Research, 01069 Dresden, Germany
[2] Institute of Materials Engineering, University of Siegen, 57076 Siegen, Germany
[3] Institute of Applied Physics, Technical University of Dresden, 01069 Dresden, Germany
[4] Institute of Materials Science, Technical University of Dresden, 01069 Dresden, Germany

Published online: 20 February 2024

1 Introduction

Temperature control is critical in modern electronics, due to the multiple effects of temperature on the performance of almost all microelectronic devices [1–3], as diverse as accuracy [4], sensitivity [5, 6], reliability [7, 8], stability [9, 10] and adjustability [11–14] of electronic components. Typically, temperature changes mainly come from diurnal and seasonal temperature variations of the external environment [15] (even a fluctuation of ~ 40 K/day or ~ 80 K/year) and the inevitable heating effect caused by operating internal high-power components (e.g., near-field wireless transmission of data [16, 17] and power [18, 19]) in the same microsystems. Moreover, the miniaturization of electronics towards high-performance and low-power consumption [20] and the diversification of demand for multidimensional integrated devices [21] in the Internet of Things make the temperature distribution of multifunctional microsystems manifest with spatial inhomogeneity and temporal uncertainty [22], leading to further challenges in thermal management [23, 24].

Heat transfer engineering is particularly important for temperature control, including passive heat transfer generally induced by a temperature difference in space, and active heat transfer driven by external physical fields [25]. To enhance solid-state thermal conduction, reducing thermal resistance [26, 27] between high-power electronics and their environment is the most widely studied passive heat dissipation strategy (demonstrated in Fig. 1a). Heat conduction can be significantly improved when combined with thermal convection using commercial fan cooling at the system level or liquid cooling at the chip level [28]. In general, two drawbacks of the above overall heat dissipation methods exist: they are not suitable for achieving local temperature stabilization at the component level; and they are limited to passively lowering the temperature difference ($\Delta T = T_s - T_a$) between the power electronics (set temperature T_s) and their environment (ambient temperature T_a). Paradoxically, lowering ΔT, in return, reduces their heat dissipation power (proportional to ΔT), resulting in poor temperature control.

Microheaters based on the Joule effect can maximize the performance of temperature-sensitive components by actively providing a stable set temperature at the microscale [10–14], which can enable a micro-electromechanical system (MEMS) resonator to achieve ppb frequency stability over external temperature variations of up to 100 K [10], and the temperature control capability can exceed 5 K mW^{-1} after increasing the thermal resistance R_{th} (as shown in Fig. 1b). While this overheating method results in increased

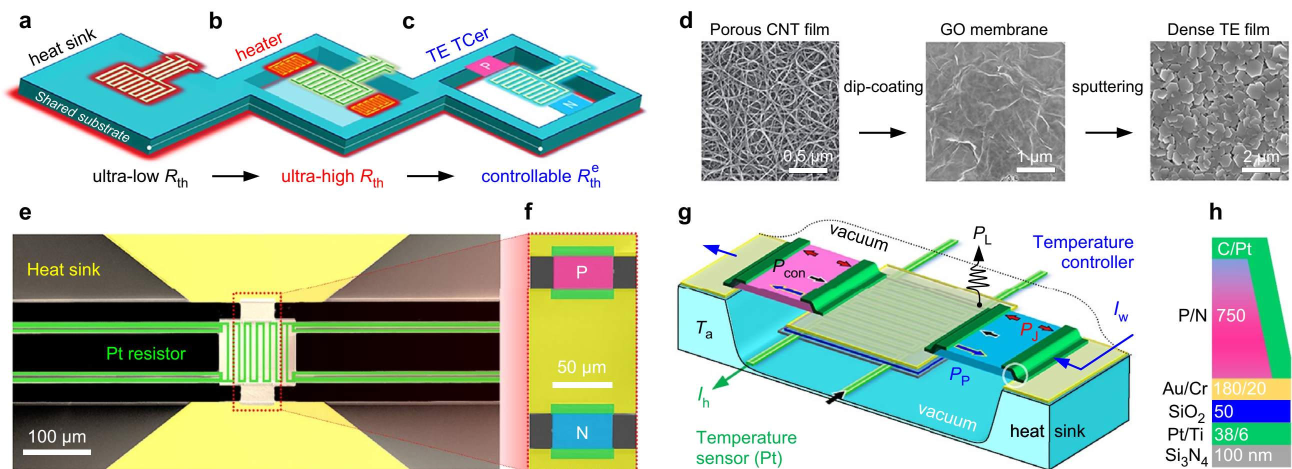

Fig. 1 Design concept of the on-chip micro temperature controllers. Schematics of temperature control through **a** cooling by a heat sink with an ultra-low intrinsic thermal resistance R_{th} for high-power electronics, **b** heating by a microheater with an ultra-high R_{th} and **c** controlling by a micro thermoelectric (TE) temperature controller with a widely controllable equivalent thermal resistance R^e_{th} for low-power electronics. Note that the heating effect in **a** mainly causes the temperature fluctuations in **b** and **c** through their shared substrate. **d** SEM images of the nanoporous carbon nanotube (CNT) film, graphene oxide (GO) nano membrane by dip-coating and dense TE film by sputtering, respectively. **e** Top view false-colour SEM image of micro temperature controller (μ-TCer), showing the lateral multilevel microstructures. **f** Close-up image of TE legs marked in **e**. **g** 3D schematic of the TCer in vacuum, composed of a TE temperature control circuit driven by working current I_w (blue arrow), and a Pt sensor to measure temperature and simulate low-power electronics using a heating current I_h (green arrow). **h** Schematic vertical multi-layer nanostructures of the μ-TCer marked with a white circle in **g**

© The authors https://doi.org/10.1007/s40820-024-01342-3

system power consumption and heat dissipation, and inevitably leads to performance degradation and shortened lifetime of electronics, this is the only on-chip temperature stabiliser available to date. Therefore, a micro temperature controller (μ-TCer) with the ability to actively control ΔT by adjusting the equivalent thermal resistance ($R_{th}^{e} = \Delta T/P_h$) for the low-power component (with heating power P_h) is highly advantageous. While intrinsic thermal resistance R_{th} is determined solely by material properties and geometry, R_{th}^{e} can be controlled by the ambient conditions (convection and radiation), active and passive heat transport in the system. In particular, R_{th}^{e} can be widely tuned by active solid-state cooling technologies based on the caloric [29] and thermoelectric [30] effects. A comprehensive comparison with the caloric coolers shows that an electronically controllable thermoelectric cooler (TEC) is more favourable owing to its stable device structure, and the advantages of not causing noise, vibration or volume changes in service. Particularly, thin-film micro TECs compatible with the integrated electronics exhibit high cooling power density and ultra-fast response [31–34].

The in-plane freestanding TEC based on nanograined SiGe films can achieve a cooling temperature of 10.3 K, but the low figure of merit of SiGe films (~ 0.14) needs to be improved [35]. A cooling temperature of up to 14 K was achieved recently by integrating high-performance Bi_2Te_3-based films with ordered microstructures into micro TECs, however, interface problems still hinder further improvement [36]. Therefore, the integration of high-performance TE nano films prepared by bottom-up strategies [37] into a micro TCer to achieve energy-efficient and wide-range temperature control for low-power components remains a major challenge. In this work, we present an on-chip μ-TCer based on a co-design concept that combines a high intrinsic R_{th} and a widely controllable R_{th}^{e} (schematically shown in Fig. 1c), enabling efficient and wide-range temperature control for low-power microelectronics. We have obtained dense and flat freestanding Bi_2Te_3-based TE nano films by sputtering technology using a newly developed ultra-thin graphene oxide membrane as a substrate (Fig. 1d), which were integrated into the μ-TCers using conventional MEMS technology (see Fig. S1 for detailed integration process). Figure 1e–h shows the structure of the μ-TCer, mainly consisting of a unicouple of 750-nm-thick n- and p-type TE legs with a length of ~ 25 μm and a width of ~ 50 μm, detailed parameters are summarized in Tables S1and S2. This optimized μ-TCer exhibits a remarkable temperature control capability of 100 K mW^{-1} and a fast response time of 5 ms, as well as excellent operational stability and cycle durability.

2 Experimental Section

2.1 Fabrication of Freestanding TE Nano Films

The carbon nanotube films prepared by vacuum filtration of carbon nanotube solution were first transferred onto SiN/Si frames (Fig. S2a−c). Then monolayer graphene oxide nanosheets were covered on carbon nanotube films by dip-coating method to form ultra-thin hybrid nano membranes (Fig. S2d, e), details in Sect. S1.1. High-purity Sb_2Te_3 (99.99%), Bi_2Te_3 (99.99%) and Bi_2Se_3 (99.99%) targets were used for co-sputtering p-type (Bi-doped Sb_2Te_3) and n-type (Se-doped Bi_2Te_3) films on above nanoporous carbon nanotube film and nanometre-thick hybrid membrane substrates, with a base chamber pressure of ~ 5.0×10^{-4} mTorr and Ar operating pressure of ~ 5 mTorr at 580 K with a ~ 30 min annealing before device integration and performance characterization. Controlling the deposition rate of the individual targets by varying the sputtering power can precisely regulate the chemical composition of the TE films.

2.2 Materials and Performance Characterization

The microstructures and phase purity of the samples were characterized by X-ray diffraction (XRD, 3000 PTS diffractometer, GE Inspection Technologies GmbH, Cu radiation) and scanning electron microscopy (SEM, Zeiss ultra55, Germany), and Energy-dispersive spectra (EDS) were used to characterize the compositions of the samples. The thicknesses of the TE films were measured by cross-sectional SEM images (Fig. S2). The standard four-probe method (LSR-3, Linseis) was used to simultaneously measure the in-plane temperature-dependent Seebeck coefficient (α) and electrical conductivity (σ) with the He gas protection from room temperature to 420 K. The power factor (PF) was calculated according to the relation $PF = \alpha^2 \times \sigma$. The measurement uncertainties for σ, α and PF were less than 2%, 5%, and 12%, respectively. The Hall electrical conductivity was measured with a physical property measurement system (PPMS) system based on the van der Pauw method, used for electrical conductivity calibration.

2.3 Integration and Measurement of Micro TCers

The fabrication process of the on-chip TE TCers is shown in Fig. S1. Beginning with a 1×1 cm^2 silicon/silicon nitride (Si/Si_3N_4) substrate, including ~300-μm-thick Si and ~100-nm-thick double-sided Si_3N_4 layers, the Si_3N_4 layer was partially etched by reactive ion etching (RIE) using CF_4 gas under the protection of the patterned photoresist. The freestanding Si_3N_4 window was obtained after removing the Si layer in the 40% KOH at 353 K for ~300 min. Second, temperature sensor electrodes (Pt/Ti, 38/6 nm, marked by green in Fig. 1e–h) were deposited on the Si_3N_4 window using standard lithography, magnetron sputtering, and lift-off process, followed by a 50-nm-thick Atomic Layer Deposition (ALD) of SiO_2 at 473 K as an insulation layer. Next, the photoresist was lithographically patterned on the SiO_2 layer, to open the electrodes for performance measurement by RIE with CF_4 gas. Third, working electrodes (Au/Cr, 180/20 nm, marked by yellow in Fig. 1e–h) can be obtained by sputtering and patterned etching. It is worth noting that the key role of the above SiO_2 layer is to insulate the Pt sensor and Au working electrodes in TCer (illustrated in the multilayer structure in Fig. 1g). Fourth, the unnecessary parts of the Si_3N_4 window together with SiO_2 are thoroughly etched by RIE with CF_4 gas to ensure good thermal insulation conditions for the μ-TCer. Finally, the individually prepared n- and p-type freestanding Bi_2Te_3-based TE thin films (Sect. 2.1) were integrated onto the above-prepared chips by the focused dual-beam technique (FEI, Helios 600i). The integrated on-chip μ-TCer is shown in the SEM image (Fig. 1e, f) and the corresponding 3D schematic (Fig. 1g, h), details in Tables S1 and S2. The PPMS system can provide a high vacuum (~0.01 mTorr) and accurate ambient temperature setting (280–380 K) for the performance test of our μ-TCers (similar to the operating temperature range of microelectronics). A Pt temperature sensor was used to assess the temperature controllability of our TCers (Fig. S3). Heat-compensation method (dual currents) was used for the cooling power and efficiency test, one is the working current (I_w), and another one is the heating current (I_h) to simulate the Joule effect of the micro components and simultaneously monitor the real-time temperature, details in Sect. S1.2.

2.4 Heat Transfer in Power Electronics

To stabilize the temperature of a low-power temperature-sensitive component in a closed system, its heating power P_h will be completely transferred to the heat sink by net cooling power P_c ($P_h = P_c$), and P_c can be described by the heat transfer equation [38]:

$$P_c = P_P - P_J/2 - P_{con} - P_L \tag{1}$$

where P_P, P_J, P_{con} and P_L are the Peltier cooling and Joule heating power, conductive heat power, and convective and radiative heat loss power, respectively. Since $P_h = P_c$ and P_L is negligible in a closed vacuum system, Eq. (1) can be expressed in detail as:

$$I_W \times T \times \alpha - I_W^2 \times R - P_h = -\Delta T / R_{th} \tag{2}$$

where I_w, T, α and R are the working current, absolute temperature, Seebeck coefficient and internal resistance of the μ-TCer, respectively. Hence, as a primary indicator of the μ-TCers for a power electronic component (with a heating current I_h), ΔT can be controlled by regulating the magnitude and direction of I_w (Fig. 2a). And its power consumption P can be expressed as [38]:

$$P = I_w^2 \times R - I_w \times \Delta T \times \alpha \tag{3}$$

Furthermore, considering that the P_c value is always equal to the P_h value, as a comprehensive evaluation index, the $R_{th}^e = \Delta T/P_h$ defined in this study can be described as:

$$R_{th}^e = \Delta T / \left(P_P - P_J/2 + \Delta T / R_{th} \right) \tag{4}$$

According to Eq. (4), R_{th}^e can be regulated by the Peltier and Joule effects, which can reflect both the temperature control range and efficiency of the μ-TCers for low-power components. In addition, we systematically analysed the effect of thermal resistances (intrinsic R_{th} and tunable R_{th}^e) on temperature control using a heat-compensation method (Sect. S1.2), including the temperature control capability ($\eta = \Delta T/P$) and coefficient of performance ($COP = P_c/P$).

© The authors https://doi.org/10.1007/s40820-024-01342-3

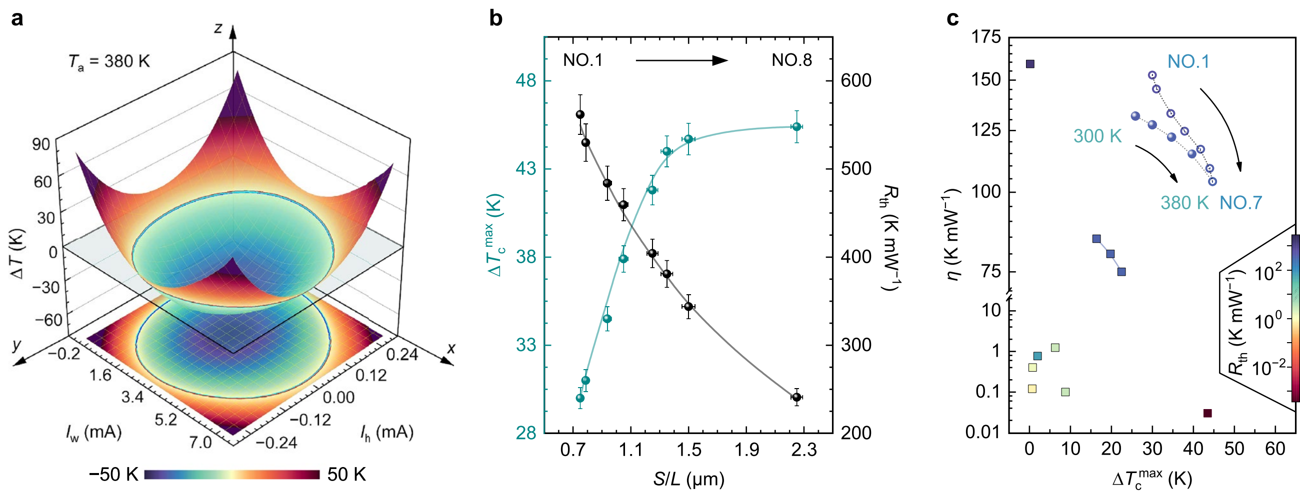

Fig. 2 Cooling performance characterization. **a** Dependence of temperature difference ΔT on working current I_w and heating current I_h of the μ-TCer with optimized geometric parameters. **b** ΔT_c^{max} (green) and R_{th} (black) as a function of the section-to-length ratio (*S*/*L*) in a series of μ-TCers (NO.1–NO.8) and their fitting lines. **c** Comparisons of cooling performance of the previously reported micro TECs (square) and μ-TCers in this work (circle), including ΔT_c^{max} ($P_c = 0$ W) and corresponding cooling temperature control capability η. Note that the colour bar indicates their intrinsic R_{th} valves, detailed data and related references are provided in Tables S1 and S3

3 Results and Discussion

3.1 Cooling for Ultra-Low Power Electronics

For an ultra-low power component ($I_h = 5$ μA and negligible $P_h < 50$ nW), the heating temperature difference continuously increases as a function of I_w from 0 to − 1 mA (Figs. 2a and S3d), due to the combined influence of Peltier and Joule effects [39]. Conversely, when I_w is reversed, the cooling temperature difference ($\Delta T_c = T_a - T_s$) decreases with an increase of I_w and reaches a minimum value before increasing (0–5 mA). Accordingly, ΔT_c is decisive for the temperature control range, which is also the unique feature that distinguishes TECs from microheaters with only a heating function.

For a comparative analysis of geometric parameter effect on the cooling performance (Fig. 2b), a series of devices with different section-to-length ratios (*S*/*L*) were fabricated (labelled NO.1–NO.9 in Tables S1 and S2). As the *S*/*L* value increases, the maximum cooling temperature difference ΔT_c^{max} increases, due to the relatively reduced effect of conductive heat loss through the Pt sensor (Fig. 1e), which was revealed by our simulations (Sect. S2 and Fig. S4). In contrast, the R_{th} value decreases as the *S*/*L* value increases because of their reciprocal relationship. As shown in Eq. (1), a large intrinsic R_{th} can suppress P_{con} for efficient cooling, therefore, the ΔT_c and R_{th} are two key parameters of the on-chip μ-TCer. Due to the small *S*/*L* of TE legs in our TCers, the ultra-high intrinsic R_{th} is two orders of magnitude higher than those of conventional TECs [40–42], resulting in extremely high η valves and greatly improved ΔT_c^{max} (detailed comparison in Fig. 2c and Sect. S3).

Since increasing ΔT_c and R_{th} to improve the temperature controllability and efficiency can not be simultaneously achieved, specific geometric parameters need to be re-designed based on practical applications. In this study, when the *S*/*L* value increases from 1.3 to 2.3 μm, the R_{th} and η valves decrease rapidly (Fig. 2b, c), but the ΔT_c^{max} value increases slowly. This is due to the local temperature rise of the heat sink in this single-stage TCer. Multi-stage cooling strategies (e.g., TECs combined with water/air cooling systems [43] and multi-stage TECs [44]) can overcome this bottleneck while reducing their efficiency [43]. Notably, they are not suitable as on-chip μ-TCer that require simple and compact structures. For comprehensive considerations, the appropriate *S*/*L* value is 1.5 μm (NO.7). The temperature-dependent ΔT_c^{max} values are shown in Fig. 3a. Specifically, it can achieve temperature differences of ~ 2 K to ~ 45 K at T_a of 100–380 K, a 100% improvement compared to flexible porous TE films with ordered microstructures [36]. For example, this on-chip μ-TCer can build and maintain a constant temperature region of 335 K for an ultra-low power

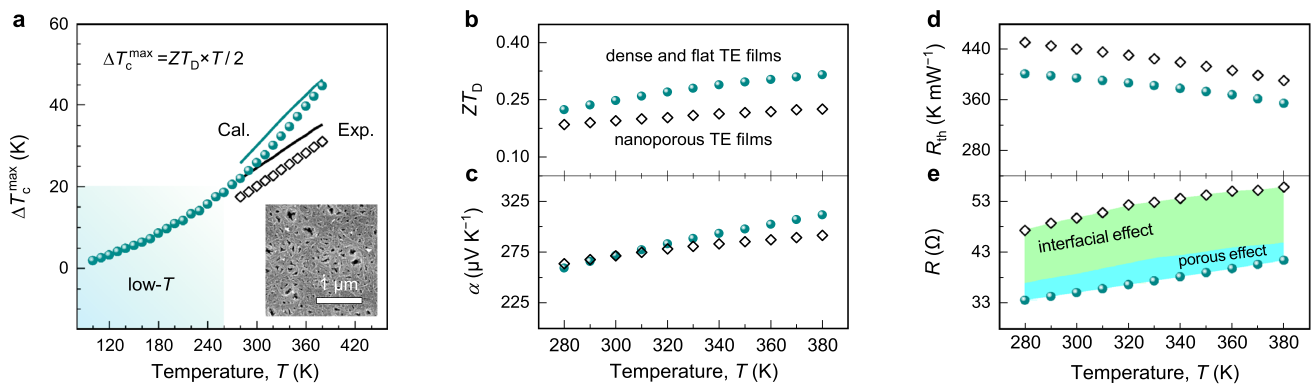

Fig. 3 Device thermoelectric performance. Temperature-dependent **a** experimental (data point) and calculated (line) maximum cooling temperature difference ΔT_c^{max}, **b** dimensionless device figure of merit ZT_D. **c** Device Seebeck coefficient α, **d** thermal resistance R_{th} and **e** internal resistance R of the μ-TCers, NO.7 with dense TE films (green) and NO.9 with porous TE films (black), respectively. The inset in **a** shows the morphological details of the porous TE films

component in a 380 K environment (Fig. S3e), making it quite suitable for the temperature control of modern microelectronics and even low-temperature electronics. Although P_L increases with working pressure, resulting in temperature control losses, the industrial ~ 10-mTorr vacuum packaging [45] can ensure temperature control losses of less than 0.5% (Sect. S4).

Figure 3 shows the temperature-dependent device TE performance of our μ-TCers, which were evaluated to explain the key role of device integration in their cooling ability. The cooling performance of the TCer (NO.7) fabricated by integrating dense and flat TE films is significantly higher than the TCer (NO.9) integrated by porous TE films (Fig. 3a). The experimental ΔT_c^{max} values for the former also match the predicted values better than the latter, based on their device figure of merit (defined as [46], $ZT_D = \alpha^2 \times R_{th}/R \times T$ in Fig. 3b). In detail, the α values of these two μ-TCers are comparable without being significantly affected by the nanoporous structure, and increase with the increasing temperature (Fig. 3c), which is consistent with the excellent performance of our TE films (Fig. S5). However, compared with R_{th} (Fig. 3d), the R value increases more significantly by ~ 40% at 300 K, due to the interface effect (~ 30%) and porous structure (~ 10% reduction in electrical conductivity, Fig. S5), mainly leading to the decrease in cooling performance (Fig. 3a). It can be concluded that the high cooling capacity should be attributed to the high performance of freestanding TE films and their high-quality integration to reduce interfacial effects, which all benefit from the improved density and flatness of the freestanding TE films. In addition, interface engineering is expected to further optimize the interface quality, thereby improving the cooling performance [47].

3.2 Temperature Control for Low-Power Electronics

For efficient directionally transferring P_h of low-power electronics while maintaining a stable control temperature, P_c is as essential as ΔT_c and R_{th} for the μ-TCer. The P_c and COP of our μ-TCer exhibit a linear relationship with ΔT (Figs. S6 and S7), which is mainly due to the P_{con} shown in Eq. (1). To further evaluate the ability of our μ-TCer to stabilize the temperature for a ~ 70-μW electronic component in a variable temperature environment, we comprehensively analysed its power consumption P calculated by Eq. (3). Figure 4a shows the P of the μ-TCer as a function of T_s and T_a, where the cyan area represents that P is less than zero, owing to its TE generation function based on the Seebeck effects [39]. The upper and lower areas close to the cyan area represent the P of TE cooling and heating, respectively. Figure 4b shows the P as a function of T_s, reaching its lowest P at a T_s of ~ 376 K (point 1, the intersection of cooling and heating P curves). The ΔT of ~ 26 K (between this T_s of ~ 376 K and T_a of 350 K) is caused by the ~ 70-μW heating effect of the component. And driven by this ΔT, this μ-TCer achieved a maximum TE power generation of 0.5 μW (comparable to the on-chip TE generators [48]), leading to a minimum P of − 0.5 μW. When this power is used for cooling or heating, P is zero, marked by the points 2 and 3 in Fig. 4b, respectively.

© The authors

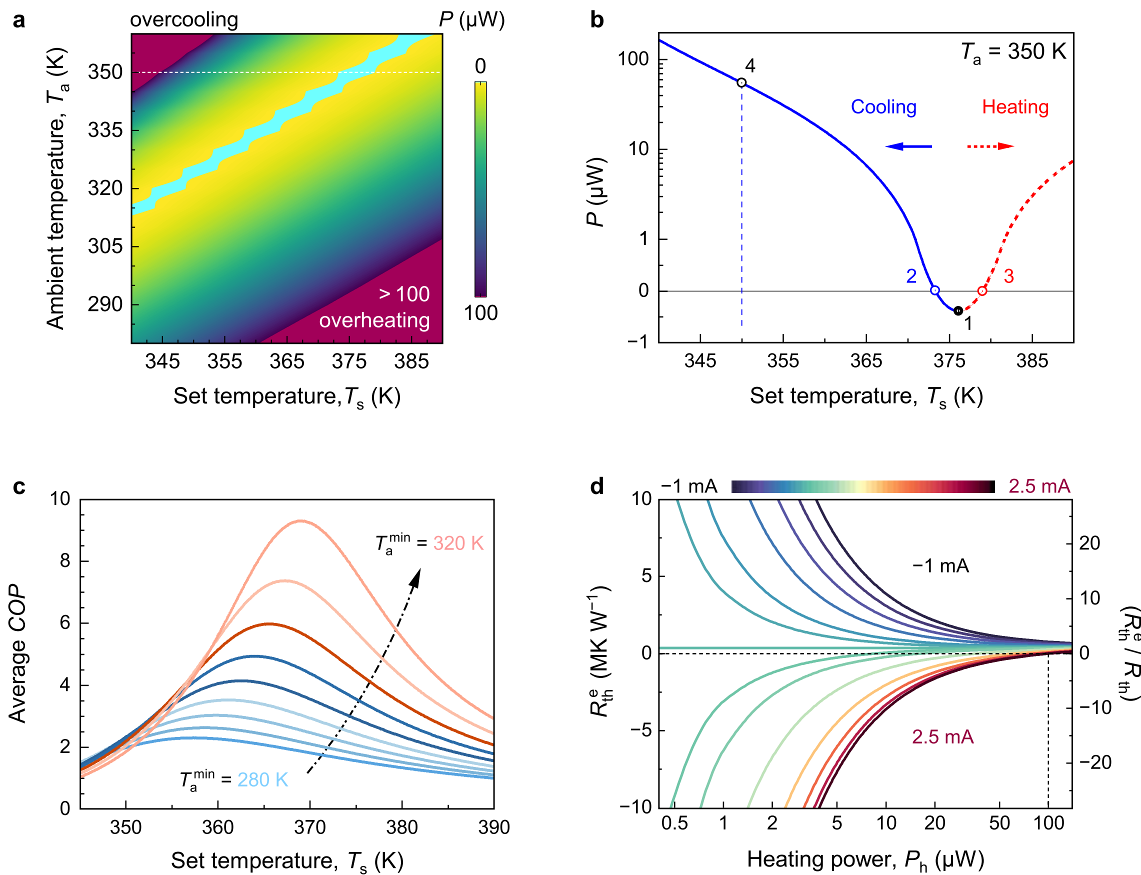

Fig. 4 Temperature control for low-power electronics. **a** Dependence of power consumption P of the thermostatic control for a ~70-μW component on T_s and T_a, detailed data in Fig. S8. **b** Power consumption P versus T_s ($T_a = 350$ K) marked by the horizontal white dotted line in **a**. **c** Average COP versus T_s over different temperature ranges from minimum ambient temperature T_a^{min} to 360 K. **d** Heating power-dependent R_{th}^e and relative thermal resistance (R_{th}^e/R_{th}) under various I_w at 350 K

To completely transfer the 70 μW P_h, a 55 μW P is required to eliminate ΔT ($T_s = T_a = 350$ K at point 4), resulting in a COP of 1.36. When T_s is below ~345 K, P increases rapidly with ΔT (T_a increases and/or T_s decreases) and even exceeds 100 μW, because of the overcooling in temperature (upper red area in Fig. 4a). Similarly, as the heating ΔT increases, P also increases rapidly because of the overheating (lower red area in Fig. 4a), which is consistent with the COP data in Figs. S7 and S8.

For the same P, the cooling temperature range is notably smaller than the heating temperature range due to the counteraction and combination of the Peltier and Joule effects (Fig. 4a). Therefore, an appropriate T_s is the key to realizing efficient temperature control for low-power electronics. To obtain the optimal T_s, the variation of the average COP ($\overline{COP}$) with T_s was summarized in Fig. 4c. In a variable temperature environment (from the minimum ambient temperature T_a^{min} to 360 K), all $\overline{COP}$s increase as T_s increases and reach their respective maximum values before starting to decrease. For instance, when the temperature range is from 280 to 360 K ($T_a^{min} = 280$ K), the lowest average P is ~30 μW (Fig. S8f), leading to an ideal $\overline{COP}$ of 2.3 (Fig. 4c), which is comparable to the COPs of most air conditioners. Moreover, as the T_a^{min} increases from 280 to 320 K, the maximum $\overline{COP}$ value increases and reaches as high as 9 in spite of the increase of optimal T_s by 10 K (Fig. 4c). Importantly, the $\overline{COP}$ of 6 could be achieved in wearable and implantable electronics because their T_a is always over 310 K, pointing us in a promising practical direction for our μ-TCers.

This μ-TCer aims at building a large and controllable R_{th}^e to minimise passive P_{con} and achieve efficient temperature control for low-power microelectronics. Figure 4d shows the results of the R_{th}^e value calculated by Eq. (4) as a function P_h under various I_w at a T_a of 350 K, the R_{th}^e value decreases

significantly as I_w increases and can be zero in cooling mode, indicating that the P_h of the microelectronic was transferred through the Peltier and Thomson effects without forming any ΔT. In particular, when I_w is zero, the R_{th}^{e} value is ~350 K mW^{-1}, which is also the intrinsic R_{th}. As I_w continues to increase, the R_{th}^{e} value becomes negative, this is the unique feature of the TE effect – transferring heat from the low-temperature side to the high-temperature side. For a ~5-μW component, the R_{th}^{e} value can be adjusted arbitrarily within the range of ±7.5 MK W^{-1} (more than ±20 times compared to intrinsic R_{th}). However, it can be seen that the lower the P_h of the microelectronic, the better the temperature controllability, which makes the μ-TCer more suitable for low-power electronics.

The widely controllable R_{th}^{e} is critical for this μ-TCer to achieve highly energy-efficient temperature control, including the multi-levels of energy savings: (1) micro-zone temperature control; (2) ultra-high thermal resistance; (3) a combination of TE cooling, heating and generation. The high intrinsic R_{th} is mainly due to the larger geometry controllability of the *S/L* (Fig. 2b) compared to other integrated TE devices [48] and the low thermal conductivity of in-plane TE films, as well as avoiding heat loss from substrates [42] and gas environment (Supplementary Sect. 4). The wide tunability of R_{th}^{e} relies on the superior ZT_D value (Fig. 3b) and the high-quality integration of dense TE films in the compact unicouple μ-TCers to reduce interfacial effects.

3.3 Controllability and Stability

To evaluate the reliability of the μ-TCer, we investigated the temperature control stability and cycling durability using an alternating I_w to drive the cooling and heating functions. Figure 5a shows that during the continuous test (including cooling and heating), the control temperature fluctuates by less than 0.1 K per cycle, and less than 0.2 K after 1000 cycles, demonstrating excellent operational stability. Note that the overall temperature variation throughout 1 h mainly comes from the fluctuating T_a instead of the changes in the control temperature, confirmed by the differences and average values of cooling and heating temperatures (Fig. S9). After excluding the effect of T_a fluctuations, the relative temperature changes of continuous operation is about 0.4% – an order of magnitude improvement over our previously reported highest value [32].

The effect of cycling number on control temperature was also characterized to further assess cycling durability and response time (Fig. 5b). The test period of ~200 ms is much longer than the time constant of the Peltier and Joule effects [49] to ensure test accuracy. The temperature change is still less than 0.2 K even after 1 million (M) cycles, showing good temperature control stability and reliability. The μ-TCer takes only ~4 ms to cool the heating zone from 380 to 350 K (T_a) and features a short response time of 5 ms to further reduce the temperature to 342 K (63.2%), and a total of 30 ms is enough to stabilize the temperature at 320 K during the whole 1 M cycles. This response time is comparable with that of the out-of-plane micro TECs [50] and several orders of magnitude shorter than that of traditional bulk TECs for commercial and academic research [51]. The average cooling rate of 2000 K s^{-1} is three orders of magnitude higher than the bulk TE coolers [33, 50], owing to its small thermal capacity and high cooling power density.

There are four factors mainly contributing to the excellent reliability: (1) the freestanding flexible films have good flexibility [52] and thus can absorb thermal stress or strain [32],

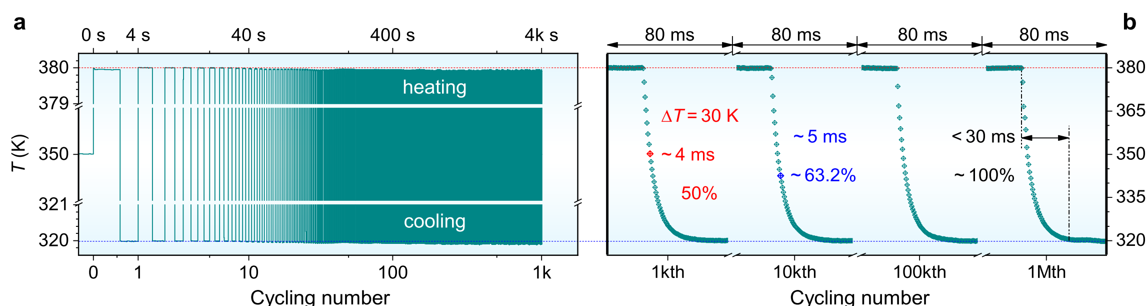

Fig. 5 Controllability and stability of the micro TE TCer. Cycling number-dependent control temperature results of the micro TE TCer using an alternating working current (−0.5/1.85 mA) for heating and cooling, respectively. **a** Continuous test results (2 s heating and 2 s cooling). **b** Intermittent test results during a single cycle (~80 ms cooling)

© The authors https://doi.org/10.1007/s40820-024-01342-3

thereby improving structural stability; (2) the simple unicouple structure makes its series circuit a lower risk of failure than a TEC containing hundreds of TE legs; (3) in contrast to the ampere-level I_w reported in the superlattice film-based [41, 53] or bulk [54, 55] TECs, the low I_w (~ 3 mA) has the advantage of generating less heat, as well as avoiding potential breakdown effects and electromagnetic interference on nearby electronics; (4) the vacuum packaging environment minimizes the chemical degradation of device material, thereby improving TE performance stability. Therefore, this μ-TCer can be used for precise temperature control of low-power temperature-sensitive electronics. It can also make an important contribution to the modulation of frequency for on-chip lasers [11, 12] and MEMS clocks [13, 14].

4 Conclusions

We report an on-chip micro temperature controller consisting of a unicouple of dense and flat freestanding TE films deposited on a newly developed ultra-thin GO nano membrane and further demonstrate its implementation in micro-zone thermal management for low-power temperature-sensitive microelectronic components. It combines the features of large intrinsic R_{th} and widely tunable R_{th}^{e} from positive to negative, leading to energy-efficient temperature control ($\overline{COP} > 2.3$ and $\eta > 100$ K mW^{-1}). The combination of Joule and Peltier effects gives it an ultra-fast cooling rate (2000 K s^{-1}) and outstanding cooling temperature difference (~ 45 K). An extremely compact device structure combined with superior reliability (> 1 M) could be important guarantees for its practical applications. In conclusion, we established an unprecedented design concept, conducted temperature control analyses of the prototype devices, proposed R_{th}^{e} as a comprehensive performance evaluation indicator. We hope that such temperature controllers can overcome emerging challenges in the ever-developing energy-efficient microelectronics.

Acknowledgements The authors thank D. Berger, D. Hofmann and C. Kupka in IFW Dresden for helpful technical support. H.R. acknowledges funding from the DFG (Deutsche Forschungsgemeinschaft) within grant number RE3973/1-1. Q.J., H.R. and K.N. conceived the work. With the support from N.Y. and X.J., Q.J. and T.G. fabricated the thermoelectric films and conducted the structural and compositional characterizations. Q.J. prepared microchips and fabricated the on-chip micro temperature controllers. Q.J. and N.P. carried out the temperature-dependent material and device performance measurements. Q.J. and H.R. performed the simulation and analytical calculations. Q.J., H.R. and K.N. wrote the manuscript with input from the other coauthors. All the authors discussed the results and commented on the manuscript.

Funding Open Access funding enabled and organized by Projekt DEAL.

Declarations

Conflict of interest The authors declare that they have no known competing financial interests or personal relationships that could have appeared to influence the work reported in this paper.

Open Access This article is licensed under a Creative Commons Attribution 4.0 International License, which permits use, sharing, adaptation, distribution and reproduction in any medium or format, as long as you give appropriate credit to the original author(s) and the source, provide a link to the Creative Commons licence, and indicate if changes were made. The images or other third party material in this article are included in the article's Creative Commons licence, unless indicated otherwise in a credit line to the material. If material is not included in the article's Creative Commons licence and your intended use is not permitted by statutory regulation or exceeds the permitted use, you will need to obtain permission directly from the copyright holder. To view a copy of this licence, visit http://creativecommons.org/licenses/by/4.0/.

Supplementary Information The online version contains supplementary material available at https://doi.org/10.1007/s40820-024-01342-3.

References

1. A.L. Moore, L. Shi, Emerging challenges and materials for thermal management of electronics. Mater. Today **17**(4), 163–174 (2014). https://doi.org/10.1016/j.mattod.2014.04.003
2. L.T. Yeh, Review of heat transfer technologies in electronic equipment. J. Electron. Packag. **117**, 333–339 (1995). https://doi.org/10.1115/1.2792113
3. K.A. Bannister, G. Giorgetti, S. Gupta, Wireless sensor networking for "Hot" applications: effects of temperature on signal strength, data collection and localization. In Proceedings of the 5th workshop on embedded networked sensors (HotEmNets' 08). (2008), pp. 1–5
4. A. Beccari, D.A. Visani, S.A. Fedorov, M.J. Bereyhi, V. Boureau et al., Strained crystalline nanomechanical resonators with quality factors above 10 billion. Nat. Phys. **18**, 436–441 (2022). https://doi.org/10.1038/s41567-021-01498-4
5. X. Xu, Q. Wang, J. Tian, L. Yang, Y. Fang et al., On the air buoyancy effect in MEMS-based gravity sensors for high resolution gravity measurements. IEEE Sens. J. **21**, 22480–22488 (2021). https://doi.org/10.1109/JSEN.2021.3106667

6. R.P. Middlemiss, A. Samarelli, D.J. Paul, J. Hough, S. Rowan et al., Measurement of the earth tides with a MEMS gravimeter. Nature **531**, 614–617 (2016). https://doi.org/10.1038/nature17397
7. V. Lakshminarayanan, N. Sriraam, The effect of temperature on the reliability of electronic components. 2014 IEEE International Conference on Electronics, Computing and Communication Technologies (CONECCT), (IEEE, Bangalore, India, 2014), pp. 1–6
8. L.T. Yeh, R.C. Chu, W.S. Janna, Thermal management of microelectronic equipment: heat transfer theory, analysis methods, and design practices. ASME press book series on electronic packaging. Appl. Mech. Rev. **56**, B46–B48 (2003). https://doi.org/10.1115/1.1566408
9. C.T.C. Nguyen, MEMS technology for timing and frequency control. IEEE Trans. Ultrason. Ferroelectr. Freq. Contr. **54**, 251–270 (2007). https://doi.org/10.1109/TUFFC.2007.240
10. L. Comenencia Ortiz, H.K. Kwon, J. Rodriguez, Y. Chen, G.D. Vukasin et al., Low-power dual mode MEMS resonators with PPB stability over temperature. J. Microelectromech. Syst. **29**, 190–201 (2020). https://doi.org/10.1109/JMEMS.2020.2970609
11. M. Corato-Zanarella, A. Gil-Molina, X. Ji, M.C. Shin, A. Mohanty et al., Widely tunable and narrow-linewidth chip-scale lasers from near-ultraviolet to near-infrared wavelengths. Nat. Photonics **17**, 157–164 (2023). https://doi.org/10.1038/s41566-022-01120-w
12. G. Liang, H. Huang, A. Mohanty, M.C. Shin, X. Ji et al., Robust, efficient, micrometre-scale phase modulators at visible wavelengths. Nat. Photonics **15**, 908–913 (2021). https://doi.org/10.1038/s41566-021-00891-y
13. W.T. Hsu, A.R. Brown, Frequency trimming for MEMS resonator oscillators. 2007 IEEE International Frequency Control Symposium Joint with the 21st European Frequency and Time Forum, (IEEE, Geneva, Switzerland, 2007), pp. 1088–1091
14. J.C. Salvia, R. Melamud, S.A. Chandorkar, S.F. Lord, T.W. Kenny, Real-time temperature compensation of MEMS oscillators using an integrated micro-oven and a phase-locked loop. J. Microelectromech. Syst. **19**, 192–201 (2010). https://doi.org/10.1109/JMEMS.2009.2035932
15. C.A. Boano, K. Römer, N. Tsiftes, Mitigating the adverse effects of temperature on low-power wireless protocols. 2014 IEEE 11th International Conference on Mobile Ad Hoc and Sensor Systems, (IEEE, Philadelphia, PA, USA, 2014), pp. 336–344
16. S. Olenik, H.S. Lee, F. Güder, The future of near-field communication-based wireless sensing. Nat. Rev. Mater. **6**, 286–288 (2021). https://doi.org/10.1038/s41578-021-00299-8
17. E. Baptista, K. Buisman, J.C. Vaz, C. Fager, Analysis of thermal coupling effects in integrated MIMO transmitters. 2017 IEEE MTT-S International Microwave Symposium (IMS), (IEEE, Honolulu, HI, USA, 2017), pp. 75–78
18. X. Lu, P. Wang, D. Niyato, D.I. Kim, Z. Han, Wireless charging technologies: fundamentals, standards, and network applications. IEEE Commun. Surv. Tutor. **18**, 1413–1452 (2016). https://doi.org/10.1109/COMST.2015.2499783
19. L. Portilla, K. Loganathan, H. Faber, A. Eid, J.G.D. Hester et al., Wirelessly powered large-area electronics for the Internet of Things. Nat. Electron. **6**, 10–17 (2023). https://doi.org/10.1038/s41928-022-00898-5
20. W. Arden, M. Brillouët, P. Cogez, M. Graef, B. Huizing et al., *More-than-Moore white paper.* (International Roadmap for Semiconductors, 2010). http://www.itrs2.net/uploads/4/9/7/7/49775221/irc-itrs-mtm-v2_3.pdf
21. Y. Zhang, F. Udrea, H. Wang, Multidimensional device architectures for efficient power electronics. Nat. Electron. **5**, 723–734 (2022). https://doi.org/10.1038/s41928-022-00860-5
22. S. Datta, W. Chakraborty, M. Radosavljevic, Toward attojoule switching energy in logic transistors. Science **378**, 733–740 (2022). https://doi.org/10.1126/science.ade7656
23. R. Mahajan, C.-P. Chiu, G. Chrysler, Cooling a microprocessor chip. Proc. IEEE **94**, 1476–1486 (2006). https://doi.org/10.1109/JPROC.2006.879800
24. Z. He, Y. Yan, Z. Zhang, Thermal management and temperature uniformity enhancement of electronic devices by micro heat sinks: a review. Energy **216**, 119223 (2021). https://doi.org/10.1016/j.energy.2020.119223
25. Y. Li, W. Li, T. Han, X. Zheng, J. Li et al., Transforming heat transfer with thermal metamaterials and devices. Nat. Rev. Mater. **6**, 488–507 (2021). https://doi.org/10.1038/s41578-021-00283-2
26. F. Tian, B. Song, X. Chen, N.K. Ravichandran, Y. Lv et al., Unusual high thermal conductivity in boron arsenide bulk crystals. Science **361**, 582–585 (2018). https://doi.org/10.1126/science.aat7932
27. K.M. Razeeb, E. Dalton, G.L.W. Cross, A.J. Robinson, Present and future thermal interface materials for electronic devices. Int. Mater. Rev. **63**, 1–21 (2018). https://doi.org/10.1080/09506608.2017.1296605
28. R. van Erp, R. Soleimanzadeh, L. Nela, G. Kampitsis, E. Matioli, Co-designing electronics with microfluidics for more sustainable cooling. Nature **585**, 211–216 (2020). https://doi.org/10.1038/s41586-020-2666-1
29. H. Hou, S. Qian, I. Takeuchi, Materials, physics and systems for multicaloric cooling. Nat. Rev. Mater. **7**, 633–652 (2022). https://doi.org/10.1038/s41578-022-00428-x
30. L.L. Baranowski, G. Jeffrey Snyder, E.S. Toberer, Effective thermal conductivity in thermoelectric materials. J. Appl. Phys. **113**, 204904 (2013). https://doi.org/10.1063/1.4807314
31. W.Y. Chen, X.L. Shi, J. Zou, Z.G. Chen, Thermoelectric coolers for on-chip thermal management: materials, design, and optimization. Mater. Sci. Eng. R. Rep. **151**, 100700 (2022). https://doi.org/10.1016/j.mser.2022.100700
32. G. Li, J. Garcia Fernandez, D.A. Lara Ramos, V. Barati, N. Pérez et al., Integrated microthermoelectric coolers with rapid response time and high device reliability. Nat. Electron. **1**, 555–561 (2018). https://doi.org/10.1038/s41928-018-0148-3
33. H. Bottner, Micropelt miniaturized thermoelectric devices: small size, high cooling power densities, short response time. ICT 2005.24th International Conference on Thermoelectrics, (IEEE, Clemson, SC, USA, 2005), pp. 1–8

© The authors

34. Q. Zhang, K. Deng, L. Wilkens, H. Reith, K. Nielsch, Micro-thermoelectric devices. Nat. Electron. **5**, 333–347 (2022). https://doi.org/10.1038/s41928-022-00776-0
35. Y. Su, J. Lu, D. Villaroman, D. Li, B. Huang, Free-standing planar thermoelectric microrefrigerators based on nano-grained *SiGe* thin films for on-chip refrigeration. Nano Energy **48**, 202–210 (2018). https://doi.org/10.1016/j.nanoen.2018.03.054
36. Q. Jin, Y. Zhao, X. Long, S. Jiang, C. Qian et al., Flexible carbon nanotube-epitaxially grown nanocrystals for micro-thermoelectric modules. Adv. Mater. **35**, 2304751 (2023). https://doi.org/10.1002/adma.202304751
37. Q. Zhu, S. Wang, X. Wang, A. Suwardi, M.H. Chua et al., Bottom-up engineering strategies for high-performance thermoelectric materials. Nano-Micro Lett. **13**, 119 (2021). https://doi.org/10.1007/s40820-021-00637-z
38. D.M. Rowe, *CRC Handbook of Thermoelectrics* (CRC Press, Boca Raton, FL, 1995)
39. L.E. Bell, Cooling, heating, generating power, and recovering waste heat with thermoelectric systems. Science **321**, 1457–1461 (2008). https://doi.org/10.1126/science.1158899
40. G.J. Snyder, J.R. Lim, C.K. Huang, J.P. Fleurial, Thermoelectric microdevice fabricated by a MEMS-like electrochemical process. Nat. Mater. **2**, 528–531 (2003). https://doi.org/10.1038/nmat943
41. G. Bulman, P. Barletta, J. Lewis, N. Baldasaro, M. Manno et al., Superlattice-based thin-film thermoelectric modules with high cooling fluxes. Nat. Commun. **7**, 10302 (2016). https://doi.org/10.1038/ncomms10302
42. Y. Chen, X. Nie, C. Sun, S. Ke, W. Xu et al., Realizing high-performance BiSbTe magnetic flexible films via acceleration movement and hopping migration of carriers. Adv. Funct. Mater. **32**, 2111373 (2022). https://doi.org/10.1002/adfm.202111373
43. J. Mao, G. Chen, Z. Ren, Thermoelectric cooling materials. Nat. Mater. **20**, 454–461 (2021). https://doi.org/10.1038/s41563-020-00852-w
44. A. Gross, G. Hwang, B. Huang, H. Yang, N. Ghafouri, et al., High-performance micro scale thermoelectric cooler: an optimized 6-stage cooler. TRANSDUCERS 2009 - 2009 International Solid-State Sensors, Actuators and Microsystems Conference, (IEEE, Denver, CO, USA, 2009), pp. 2413–2416
45. R.N. Candler, W.-T. Park, H. Li, G. Yama, A. Partridge et al., Single wafer encapsulation of MEMS devices. IEEE Trans. Adv. Packag. **26**, 227–232 (2003). https://doi.org/10.1109/TADVP.2003.818062
46. G.S. Nolas, J. Sharp, H.J. Goldsmid, *Thermoelectrics: Basic Principles and New Materials Developments* (Springer, Berlin, Heidelberg, 2001)
47. L. Yin, F. Yang, X. Bao, W. Xue, Z. Du et al., Low-temperature sintering of Ag nanoparticles for high-performance thermoelectric module design. Nat. Energy **8**, 665–674 (2023). https://doi.org/10.1038/s41560-023-01245-4
48. F. Kim, S.E. Yang, H. Ju, S. Choo, J. Lee et al., Direct ink writing of three-dimensional thermoelectric microarchitectures. Nat. Electron. **4**, 579–587 (2021). https://doi.org/10.1038/s41928-021-00622-9
49. E. Younes, J. Christofferson, K. Maize, A. Shakouri, Short time transient behavior of *SiGe*-based microrefrigerators. MRS Online Proc. Libr. **1166**, 106 (2009). https://doi.org/10.1557/PROC-1166-N01-06
50. H. Bottner, J. Nurnus, A. Gavrikov, G. Kuhner, M. Jagle et al., New thermoelectric components using microsystem technologies. J. Microelectromech. Syst. **13**, 414–420 (2004). https://doi.org/10.1109/JMEMS.2004.828740
51. V.A. Semeniouk, T.V. Pilipenko, Thermoelectric coolers with small response time. Fifteenth International Conference on Thermoelectrics. Proceedings ICT '96, (IEEE, Pasadena, CA, USA, 2002), pp. 301–306
52. Q. Jin, S. Jiang, Y. Zhao, D. Wang, J. Qiu et al., Flexible layer-structured Bi_2Te_3 thermoelectric on a carbon nanotube scaffold. Nat. Mater. **18**, 62–68 (2019). https://doi.org/10.1038/s41563-018-0217-z
53. R. Venkatasubramanian, E. Siivola, T. Colpitts, B. O'Quinn, Thin-film thermoelectric devices with high room-temperature figures of merit. Nature **413**, 597–602 (2001). https://doi.org/10.1038/35098012
54. J. Mao, H. Zhu, Z. Ding, Z. Liu, G.A. Gamage et al., High thermoelectric cooling performance of n-type Mg_3Bi_2-based materials. Science **365**, 495–498 (2019). https://doi.org/10.1126/science.aax7792
55. Z. Liu, W. Gao, H. Oshima, K. Nagase, C.H. Lee et al., Maximizing the performance of n-type Mg_3Bi_2 based materials for room-temperature power generation and thermoelectric cooling. Nat. Commun. **13**, 1120 (2022). https://doi.org/10.1038/s41467-022-28798-4